Dependence of Earth Pressures on Displacements

Pressions de Terres en Fonction des Déplacements

S.VIDMAR Professor,
B.MAJES Assistant, Civil Engineering Department, University of Ljubljana, Yugoslavia

SYNOPSIS In a model kid the earth pressures were observed corresponding to increasing translatory movements of the supporting rigid plate in passive direction. The measured earth pressures have been compared with computed values obtained by a successive use of the finite element method. The deformability of the soil was investigated by triaxial tests and expressed by families of octahedral strain versus octahedral stress charts. The infinite increase of shear strains at constant volume appearing at stress states approaching the failure had been taken into account. Tests were performed with increasing shear stresses at different constant values of the octahedral normal stress, the succession of the later corresponding to the first loading as occurring in the case of the passive pressure. The degree of the strength mobilisation in successive displacement stages has been presented by lines of equal moduli of shear deformation (G); the lines $G \to 0$ indicate the failure zones.

INTRODUCTION

The measurements of earth pressures on small models can give qualitative and quantitative insight into the mutual relationships between the forces acting on the supporting plate and the displacement of the plate. Owing to the complexity of the model scales the results cannot directly be applied for predicting earth pressures affecting high structures. They are, however, useful for checking the ability of computation methods forecasting the earth pressures as depending on the kinematical boundary conditions as well as on the deformability and strength of the background soil.

The dependence of earth pressures on kinematic boundary conditions had been experimentally investigated by several authors. The conclusions had, however, to be limited to immediate deductions from experimental data.

Recently, some interesting comparisons between measured and computed earth pressures have been published. Simpson and Wroth (1972) have used the state boundary method applying the finite element method. James et al (1972) have applied the method of characteristics of Sokolovsky, Shield's equations and experimentally obtained stress-strain relationships. Šuklje et al (1968) interpreted Vidmar's (1963) experimental observations of relaxation effects in a viscous background by an approximate computation procedure taking into account non-linear and viscous deformability as observed in triaxial compression tests.

Clough and Duncan (1971) have used the finite element method expressing the stress-strain relationships as observed in triaxial compression tests by Kondner's hyperbolic function.

In the present report some earth pressures previously measured in a model kid (Vidmar 1974-b) are compared with the computed values as obtained by the finite element method using the triaxial compression test data. The deformability of the soil has been expressed by two families of charts relating moduli of compressibility and moduli of shear deformations to the octahedral values of strains.

STRESS-STRAIN RELATIONSHIPS

The model kid was filled with a sandy silt of intermediate plasticity (MI according to AC classification; grain-size distribution: 2% < 0,002, 53% 0,002/0,06, 45% 0,06/2,0, w_L = 46%, I_P = 18%). The initial water content of the fill was w_{in} = 26,5%.

The deformability of the soil was investigated on a single triaxial specimen with initial water content w_{in} = 32,3%. The stress path of the whole drained test

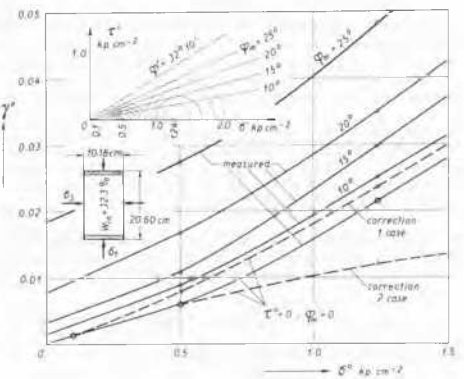

Fig. 1 Stress path of the drained triaxial test and $\gamma^o = [\gamma^o(\sigma^o)]_{\varphi_m = \text{const}}$ charts

is shown in Fig. 1. After the isotropic consolidation at spheric stresses $\sigma_1=\sigma_2=\sigma_3=$ 0,1 and 0,5 kp cm^{-2} the stress level was successively raised to the straigt envelopes $\tau=\sigma'\tan\varphi_m$ of Mohr's stress-circles at $\varphi_m=$ = 10°, 15°, 20° and 25°. The unloading occurred at the reversal succession of the same stress states. Then the spheric stress 0,5 kp cm^{-2} was increased to 1,24 kp cm^{-2} and, keeping this value constant, the shear stresses were raised again to previously chosen levels. Settlements of the sample and volume changes were registered during each loading step up to the end of the primary consolidation. As the secondary effects had not been found important, the last readings in each step were considered when computing the octahedral values of normal (ε°) and shear (γ°) strains corresponding to the octahedral values of effective normal (σ'°) and shear stresses (τ°) determining the stress state:

$$\varepsilon_{oct} \equiv \varepsilon^\circ = \frac{\varepsilon_v}{3} \quad \ldots\ldots\ldots\ldots\ldots (1)$$

$$\gamma_{oct} \equiv \gamma^\circ = \frac{\sqrt{2}}{3}(3\varepsilon_1 - \varepsilon_v) \quad \ldots\ldots\ldots (2)$$

$$\sigma_{oct} \equiv \sigma^\circ = \frac{1}{3}(\sigma'_1 + 2\sigma'_3) \quad \ldots\ldots\ldots (3)$$

$$\tau_{oct} \equiv \tau^\circ = \frac{\sqrt{2}}{3}(\sigma_1 - \sigma_3) \quad \ldots\ldots\ldots\ldots (4)$$

ε_1 = axial strain, ε_v = volume strain

The measured values of γ° at three normal octahedral stresses for the above mentioned values of φ_m are shown in Fig. 1.

By using experimental data, two families of stress–strain charts were formed:

$$\sigma^\circ = [\sigma^\circ(\varepsilon^\circ)]_{\gamma^\circ=\text{const}} \quad \ldots\ldots\ldots\ldots (5)$$

and

$$\tau^\circ = [\tau^\circ(\gamma^\circ)]_{\varepsilon^\circ=\text{const}} \quad \ldots\ldots\ldots\ldots (6)$$

Thereby, two alternative corrections were made when forming the charts (6). In the first case the γ° values observed at σ° = 0,5 and 1,24 kp cm^{-2} were increased by the amount of the irrecoverable shear strain which would appear at σ° = 0,1 kp cm^{-2} if the deviatoric loading and unloading was realized also at this value of σ°; the amount had been estimated by extrapolating the available test data (see Vidmar 1974-b and Fig. 1). In the second case the γ° values at σ° = 1,24 kp cm^{-2} were decresed by the irrecoverable shear strain observed at σ° = 0,5 kp cm^{-2}. With this alternative correction the charts (6) can be considered to correspond to three separate test series in which the deviatoric loading was not preceded by any deviatoric stress path.

For the charts (5) and (6) according to the first of the above mentioned correction we refer to a previous publication (Vidmar 1974-a). The family of the charts (6) according to the second of the above mentioned correction is presented in Fig. 2.

By using the charts (5) and (6), secant values of the moduli of compressibility (K) and moduli of shear deformation (G) were obtained according to the relations

$$K = \frac{1}{3}\frac{\Delta\sigma^\circ}{\Delta\varepsilon^\circ}, \quad G = \frac{\Delta\tau^\circ}{\Delta\gamma^\circ} \quad \ldots\ldots\ldots (7),(8)$$

The resulting values have given the charts

$$K = [K(\varepsilon^\circ)]_{\gamma^\circ=\text{const}} \quad \ldots\ldots\ldots\ldots (9)$$

and

$$G = [G(\gamma^\circ)]_{\varepsilon^\circ=\text{const}} \quad \ldots\ldots\ldots\ldots (10)$$

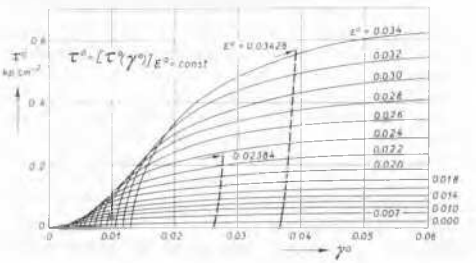

Fig. 2 Charts $\tau^\circ = [\tau^\circ(\gamma^\circ)]_{\varepsilon^\circ=\text{const}}$

which are presented in Figs. 3 and 4. When approaching failure, the moduli of shear deformation G get zero values. According to the data of three direct shear tests, the failure stress level was taken with φ_m = = φ' = 32° 10'; thereby the cohesion intercept of about

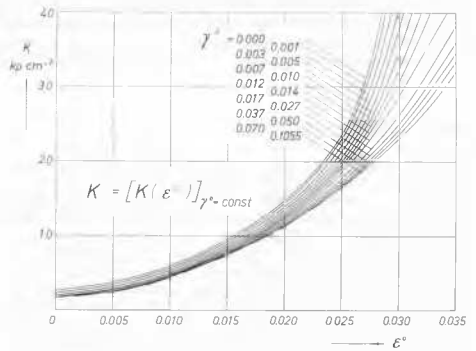

Fig. 3 Charts $K = [K(\varepsilon^\circ)]_{\gamma^\circ=\text{const}}$

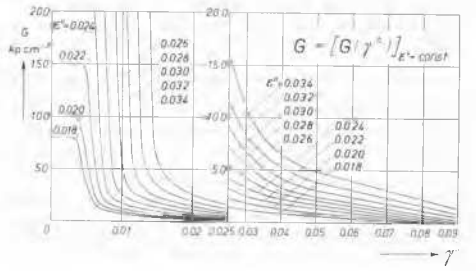

Fig. 4 Charts $G = [G(\gamma^\circ)]_{\varepsilon^\circ=\text{const}}$
$0{,}018 < \varepsilon^\circ < 0{,}034$

0,06 kp cm^{-2} at w_{in} = 32,3% and of 0,12 kp cm^{-2} at w_{in} = 26,5% had been disregarded.

The relationships (9) and (10) have been expressed by sets of numerical coordinate values according to Figs. 3 and 4. The interpolation was made by applying the

"spline" polynomials of the third order. The computation program was elaborated according to Desai (1972).

COMPUTATION OF PASSIVE EARTH PRESSURES

With the geometric and loading conditions of the model tests (for details see Vidmar 1974-b) and the stress-strain relationships of triaxial test presented in the preceding section, the passive earth pressures were computed by using the finite element method. The background of the model was 23 cm in height, 21,3 cm in width and 180 cm in length; it was subjected to a flexible surface load of $q = 0,096$ kp cm^{-2} 80 cm in length and, after the consolidation under this load, to lateral forces producing a translatory movement of the rigid metal supporting plate. In the numerical computation the background was considered a plane-strain body discretizated into a network of triangular finite elements according to Fig. 5. The assumptions on the kinematical boundary conditions are shown in the figure.

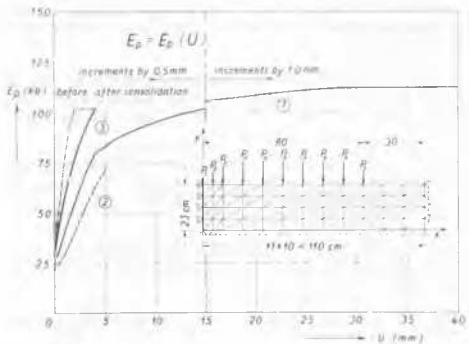

Fig. 5 The network of finite elements in the background with the boundary conditions and plots of total earth pressures E versus displacements U of the supporting plate: (1) computed values according to charts presented in Figs. 3 and 4, $w_{in} = 32,3\%$; (2) computed values according to charts presented by Vidmar 1974-a, $w_{in} = 32,3\%$; (3) measured values, $w_{in} = 26,5\%$

The non-linear stress-strain relationships for the soil were linearized by the incremental procedure; the loads and boundary displacements respectively were devided into a succession of small increments.

The numerical computation occurred in the following three phases:

(1) step loading by the own weight of the soil at the fixed position of the supporting plate;
(2) step loading by the surface forces, the supporting plate remaining fixed;
(3) incremental translatory movement of the supporting plate, the surface loading remaining constant.

At the very beginning of the procedure $\sigma^\circ = \tau^\circ = \varepsilon^\circ = \gamma^\circ = 0$ in each finite element, and K and G values are equal for any element. The corresponding "elastic" parameters E and ν (modulus of linear deformation and Poisson's ratio) can be obtained by the relations:

$$\nu = \frac{3K - 2G}{2(3K + G)}, \quad E = 2G(1 + \nu) \ldots\ldots (11),(12)$$

The stress and strain increments have been successively added to preceding values in order to get stress and strain tensors at the end of the increment. The corresponding octahedral values

$$\varepsilon^\circ = \frac{J_1}{3}, \quad \gamma^\circ = 2\sqrt{\frac{2}{3}}\sqrt{\frac{J_1^2}{3} - J_2} \ldots\ldots (13),(14)$$

have been obtained by taking into account that for plane strain conditions the strain invariants J_1 and J_2 are:

$$J_1 = \varepsilon_{xx} + \varepsilon_{yy}, \quad J_2 = \varepsilon_{xx}\varepsilon_{yy} - \left(\frac{\gamma_{xy}}{2}\right)^2 \ldots\ldots (15),(16)$$

By using "spline" subroutine the tangent moduli $K = K(\varepsilon^\circ, \gamma^\circ)$ and $G = G(\gamma^\circ, \varepsilon^\circ)$ may be obtained. The corresponding E and ν values obtained from equations (11) and (12) have to be inserted into the stiffness and "elastic" matrices of the following step. When approaching the failure, G = 0 has to be substituted by a very small value (e.g. $G = 10^{-10}$ kp cm^{-2}) and $\nu = 0,5$ by a smaller adjacent value (e.g. $\nu = 0,499$) in order to avoid singularity of the stiffness matrix.

RESULTS OF THE NUMERICAL ANALYSIS AND COMPARISON WITH MEASURED VALUES

Distribution of earth pressure (σ_{xx}) along the height of the supporting plate is presented in Fig. 6, and the integrated values of total earth pressures are plotted versus the displacement of the plate in Fig.5.

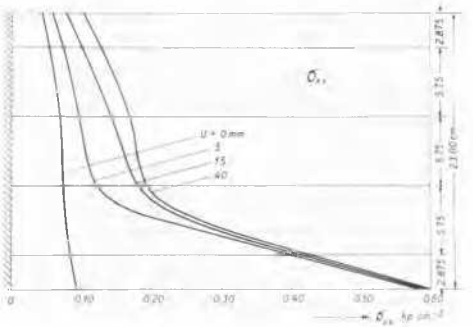

Fig. 6 Distribution of earth pressures along the height of the plate as depending on the displacement U of the plate

In Fig. 5 the resulting total pressures have been compared with the computed values which have been previously obtained by the author (Vidmar 1974-a). In the same figure the observed values have been presented as well. (For details see Vidmar 1974-b). The horizontal movement of the plate occurred at the speed of 0,00083 mm sec^{-1}. After a displacement of 2 mm the observed initial at rest pressure of 30,3 kp increased up to 102 kp. At this pressure kept constant the displacement increased, during the primary consolidation, in about 5.10^3 min up to about 4 mm and at the end of observation, in 13.10^3 min, up to about 4,5 mm. The interruption of line 1 at U = 15 mm is owned to different values of increments ΔU at displacement $0 < U < 15$ mm and $U > 15$ mm.

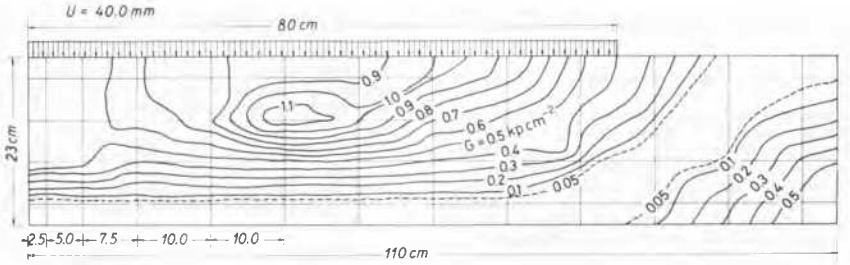

Fig. 7 Isobares of moduli G related to the displacement of U = 40 mm

In the domain of the observed displacements (< 4,5mm) the measured earth pressures in the consolidated state (full line 3 in Fig. 5) are by about 20% higher than the computed values (line 1). The difference may be owned mainly to different initial water contents of the soil in the model kid and of the triaxiel specimen (26,5% against 32,3%), and to the correspondingly higher cohesion intercept (0,13 versus 0,06 kp cm^{-2}) which was not considered at all in the numerical analysis. On the other hand, since in the $G = G(\gamma^c, \varepsilon^c)$ relationships the deviatoric unloading was not taken into account, even greater difference between measured and computed values could be expected. This is proved by smaller earth pressures obtained by the author when using the stress-strain relationships according to the first alternative correction (line 2 in Fig. 5). Neither of the alternative procedure, however, follows exactly the stress path at the transition from at rest pressure through the hydrostatic stress state in the domain of passive pressures.

In Fig. 7 the isobares of the moduli G have been presented. They are related to the displacement of U = 40 mm when between the isobares 0,05 a clearly formed failure zone appeared.

CONCLUSIONS

The above comparison between computed and measured passive earth pressures has proved the ability of numerical computation method to forecast the earth pressures with satisfactory approximation provided that the stress-strain relationships had been taken into account in the correct way. They do not need to be expressed in analytical form; they may be presented by a set of point values and the interpolation may be made by using "spline" functions. The hypoelastic presentation of soil properties as applied in the paper could, however, be improved (1) by deducing the rheological relationships from the plane-strain triaxial tests, (2) by applying unloading (elastic) moduli G during the transition from the at rest state to the spheric stress state, (3) by a better approach to the stress history of the triaxial sample, (4) by considering the effect of viscous soil properties (see Vidmar 1963 and 1974-b). According to recent studies (e.g. Lade 1975, Lade and Musante 1976, Prévost and Höeg 1976) elasto-plastic soil models provide further improvement of the analysis.

ACKNOWLEDGEMENT

The authors wish to express their thanks to Professor L. Šuklje, University of Ljubljana, Yugoslavia, for his helpful suggestions and useful advice during preparation of this paper.

The investigations dealt with in the paper have been financed by the Boris Kidrič Fund, Ljubljana.

REFERENCES

Clough, G.W. and J.M. Duncan (1971), "Finite Element Analysis of Retaining Wall Behaviour," Journal of the Soil Mechanics and Foundation Division, Proc. of ASCE, pp. 1657-1673.

Desai, C.S. (1972), "Theory and Application of the Finite Element Method in Geotechnical Engineering," Proc. of the Symposium held at Vicksburg, Mississippi, pp. 3-90.

James, R.G. et al (1972), "The Prediction of Stresses and Deformations in a Sand Mass Adjacent to a Retaining Wall," Proc. 5th Eu. Conf. S.M.F.E., Vol. 1, pp. 39-47.

Lade, P.V. (1975), "Elasto-Plastic Stress-Strain Theory for Cohesionless Soil with Curved Yield Surface," UCLA - ENG - 7594, 97 pp.

Lade, P.V. and H.M. Musante (1976), "Three-Dimensional Behaviour of Normally Consolidated Cohesive Soil," UCLA - ENG - 7626, 166 pp.

Prévost, J.H. and K. Höeg (1975), "Soil Mechanics and Plasticity Analysis of Strain Softening," Geotechnique, Vol. 25, No. 2, pp. 279-297.

Simpson, B. and C.P. Wroth (1972), "Finite Elements Computations for a Model Retaining Wall in Sand," Proc. 5th Eu. Conf. S.M.F.E., Vol. 1, pp. 85-95.

Šuklje, L. et al (1968), "Dependence of Earth Pressures on Strains in Rankine's Case," Acta Geotecnica, University of Ljubljana, No. 21-23, 19 pp.

Vidmar. S. (1963), "Relaxation Effects on the Earth Pressures of Cohesive Soils," Proc. Int. Conf. S.M.F.E, Budapest, pp. 103-118.

Vidmar, S. (1974-a), "Contribution to the Discussion," Proc. 4th Danube-European Conf. S.M.F.E., Vol. 2, pp. 67-68.

Vidmar, S. (1974-b), "Earth Pressures onto the Rigid Construction as Depending on Kinematic Boundary Conditions," Thesis, University of Ljubljana, Civil Engineering Department, 108 pp.